Journal of Biomechanics 96 (2019) 109357

Contents lists available at ScienceDirect

Journal of Biomechanics

journal homepage: www.elsevier.com/locate/jbiomech
www.JBiomech.com

Torsional motion of the left ventricle does not affect ventricular fluid dynamics of both foetal and adult hearts

Vivek Vasudevan [1], Hadi Wiputra [1], Choon Hwai Yap *

Department of Biomedical Engineering, National University of Singapore, Singapore

ARTICLE INFO

Article history:
Accepted 18 September 2019

Keywords:
Left ventricle
Adult porcine
Human foetal
Torsion
Twist
Computational fluid dynamics
Intra-cardiac fluid mechanics

ABSTRACT

Left ventricular torsion is caused by shortening and relaxation of the helical fibres in the myocardium, and is thought to be an optimal configuration for minimizing myocardial tissue strains. Characteristics of torsional motion has also been proposed to be markers for cardiac dysfunction. However, its effects on fluid and energy dynamics in the left ventricle have not been comprehensively investigated. To investigate this, we performed image-based flow simulations on five healthy adult porcine and two healthy human foetal left ventricles (representing two different length scales) at different degrees of torsional motions. In the adult porcine ventricles, cardiac features such as papillary muscles and mitral valves, and cardiac conditions such as myocardial infarctions, were also included to investigate the effect of twist. The results showed that, for all conditions investigated, ventricular torsional motion caused minimal changes to flow patterns, and consistently accounted for less than 2% of the energy losses, wall shear stresses, and ejection momentum energy. In contrast, physiological characteristics such as chamber size, stroke volume and heart rate had a much greater influence on flow patterns and energy dynamics. The results thus suggested that it might not be necessary to model the torsional motion to study the flow and energy dynamics in left ventricles.

1. Introduction

The helical structure of fibres in the myocardium and the change in angles of these fibres along the myocardial wall thickness leads to torsional motion of the ventricle during contraction and relaxation (Sengupta et al., 2007; Taber et al., 1996). Torsional motion is the circular movement of the left ventricle (LV) about its long axis, and is typically anti-clockwise from the superior view from the base of the heart. Typically, the apex and the base rotate in opposite directions, and torsion is assessed by the angular difference of rotation between them. In a normal heart, this torsional coiling motion develops during ejection, and the subsequent uncoiling sets the stage for rapid filling after the isovolumic post-ejection interval (Buckberg et al., 2015). The extent of LV twisting is correlated with ejection fraction and longitudinal deformations of the heart (Pacileo et al., 2011), since both the torsion and stroke volume originate from myocardial contractions. Based on solid mechanics studies, coiling of the myocardium was proposed to be optimised for a uniform distribution of stress and minimal strain per ejected volume (Grosberg and Gharib, 2009), and systolic ventricular torsion was proposed to be a storage of elastic potential energy that would assist in diastole recoil untwisting (Nakatani, 2011).

This torsional motion of the LV has been proposed as a marker for LV diseases. Torsion is a good indicator of the state of LV contraction and relaxation, and its characteristics change during LV dysfunction. For example, patients with various forms of cardiomyopathy were observed to have lower twist rate, and delayed onset of untwisting (Pacileo et al., 2011). Patients with heart failure with normal ejection fraction have been observed to have reduced LV apical rotation, and delayed untwisting, which coincided with reduced LV suction and high end-diastolic pressures (Tan et al., 2009).

To date, however, the effect of LV torsion on the intra-cardiac fluid dynamics has not been comprehensively characterized. Conceivably, the twist motion would induce a flow tangential to the LV wall due to viscous effects, but its exact contribution to flow patterns, fluid kinetic energy and work done for systolic ejection need to be quantified. Multiple authors have utilized computational fluid dynamics (CFD) simulations to assess the fluid and energy dynamics in the heart (Lai et al., 2016; Seo et al., 2014; Vedula et al., 2016; Wiputra et al., 2016), and were successful in improving our understanding of ventricular fluid dynamics. However, these studies did not include LV twist, and it remains unclear

* Corresponding author.
E-mail address: bieyapc@nus.edu.sg (C.H. Yap).
[1] Authors have equal contributions.

https://doi.org/10.1016/j.jbiomech.2019.109357
0021-9290/

if this would cause significant errors. LV fluid mechanics during diastole is characterized by vortex rings brought about by mitral inflow (Domenichini et al., 2005; Elbaz et al., 2014; Pedrizzetti et al., 2014). These vortices are known to play a crucial role in LV fluid and energy dynamics. It would also be of interest to understand if LV twist has an effect on these vortices.

In the current study, we performed CFD simulations based on in vivo images to evaluate the effect of LV twist on intra-cardiac fluid and energy dynamics. We investigated adult and foetal hearts, which were at different size scales, and investigated cases in the presence and absence of papillary muscles and mitral valves. Additionally, we also investigated cases which had cardiac abnormalities such as myocardial infarction. The results indicated that, for all cases investigated, the effects of LV torsion on fluid and energy dynamics were negligible.

2. Methodology

The effects of LV twist were investigated at two different length scales: two 22-weeks old human foetal LVs and five adult porcine LVs. All intervention and imaging experiments in animals were reviewed and approved by the Institutional Animal Care and Use Committee (IACUC) at The National University of Singapore, while all human subject imaging was approved by the Domain Specific Review Board at the National University Heath Systems.

2.1. Porcine animal model and MRI acquisition

Five healthy adult porcine animals were scanned with a 3 T Skyra MRI System (Siemens Medical Solutions, Erlangen, Germany) scanner. Multi-phase gated cine images were acquired for several short-axis and three long-axis slices to cover the porcine heart. For each scan, 25 cine-images were captured per cardiac cycle, at an in-plane resolution of $1.66 \times 1.66\ mm^2$ and a through-plane resolution of 10 mm. Myocardial infarction (MI) was induced in two of the porcine subjects through permanent ligation of left circumflex coronary artery (LCx). MR imaging scans were then performed at 2 additional time points: one week (acute, "W_1") and 4 weeks (chronic, "W_4") post-LCx.

2.2. Human foetal heart and ultrasound acquisition

4D Ultrasound images were acquired under the Spatio-Temporal Image Correlation (STIC) mode during routine checks at 22nd week of gestation, using the Voluson 730 ultrasound machine with RAB 4-8L transducer (General Electric, Connecticut, USA). Images provided 29 – 37 vol images per cardiac cycle, which could be extracted using 4DView software (General Electric, Connecticut, USA) into a stack of 29 cine-image slices, spaced 0.7 mm apart.

2.3. 3D reconstruction of pocine adult and human foetal LVs

Reconstruction of the porcine LV model at each time point of the cardiac cycle was performed in Vascular Modelling Toolkit (VMTK, www.vmtk.org) via a level set segmentation algorithm. Papillary muscles were included in one of the porcine LVs by taking care to preserve them during the segmentation and smoothing process. The 3D LV surfaces were smoothed with Geomagic Studio® (Geomagic Inc., Morrisville, NC, USA). For cases which excluded the papillary muscles, the features were removed by smoothing the LV wall. For human foetal LVs, the ultrasound images were first segmented via semi-automatic lazy-snapping algorithm (Li et al., 2004), before reconstruction and surface smoothing as in the adult porcine case. The noisy ultrasound data prevented identification of the papillary muscles and, hence, these cardiac features were excluded from the foetal hearts during segmentation.

2.4. Mathematical modelling of LV wall motion

Mathematical modelling of LV wall motion were performed using previously established methods (Lai et al., 2016; Vasudevan et al., 2017; Wiputra et al., 2016) and greater details of methods and limitations are discussed in these earlier publications. Briefly, a spherical coordinate system was employed from the centroid of the LV volume, with θ and ϕ as the angle coordinates and r as the radial coordinates (Fig. 1). The LV wall motion was described as a combination of two motions: motion in the radial direction (r) towards/away from the centroid, and motion in the azimuthal direction (θ) perpendicular to the radial axis, corresponding to the twist of the ventricle. The extent of twist motion (γ) was assumed to vary linearly with the polar angle coordinate (ϕ) from the apex to the base of the heart. Further details are available in supplementary text.

2.5. Mathematical modelling of mitral valve (MV) motion

The MV geometry was based on detailed anatomical measurements from a database of 10 adult porcine specimens (Kunzelman et al., 1994), and motion modelling was based on our previous study (Vasudevan et al., 2019). Details are available in the supplementary text. The digitally reconstructed MV was then inserted into the reconstructed porcine LV model (Fig. S1a–c). The motion of MV leaflets was prescribed based on the measurement of leaflet opening angles (angles between the leaflets and the mitral orifice plane) in the 3-chamber view from MRI data (Fig. S1d). During the cardiac cycle, the leaflets were modelled to fold along axes tangential to the prescribed orifice contour at the aforementioned angles. A foetal mitral valve was modelled by scaling down this adult mitral valve model and then inserted into the reconstructed foetal LV.

2.6. Computational fluid dynamics (CFD) simulation

Dynamic mesh CFD simulations were performed with the ANSYS Workbench Suite (ANSYS, Inc., Canonsburg, PA, USA), using

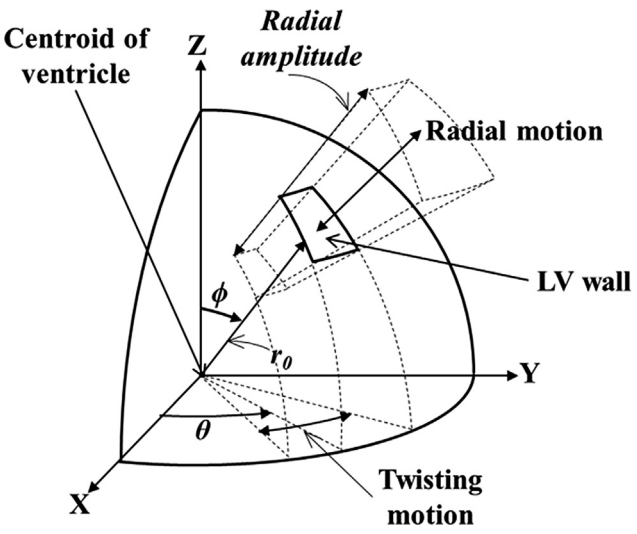

Fig. 1. Schematic to demonstrate the spherical coordinate system employed for modelling ventricular wall motion and its relationship to the cartesian coordinate system. Schematic also indicates the ventricular wall motions modelled, which were the radial motion (towards/away from the centroid), and the twisting motion (motion in the θ direction, perpendicular to the direction of radial motion).

previous established methodology (Vasudevan et al., 2019). User-defined functions (UDFs) were employed to specify motions of ventricular wall and mitral valve leaflets. Simulations were performed for four cardiac cycles so as to remove any artefacts of the stagnant initial condition, and results from the fourth cardiac cycle were used for analysis. Details of methods, including boundary conditions and mesh convergence study results, are given in the supplementary text.

In order to assess the effects of torsion on LV fluid dynamics, simulations were performed at various degrees of twist. For the foetal cases, there is a lack of torsion data in literature, and as such, we adopted twist data for neonates and toddlers, found to be about $\varepsilon = 2–5^{\circ}$ (Zhang et al., 2010). However, we simulated peak apical twist values (ε) of 0°, 5°, 10° and up to 15°, which was close to 8 times that found in neonates (Zhang et al., 2010). The more extreme case of $\varepsilon = 15^{\circ}$ was investigated so as to more firmly prove lack of influence of torsional motion on flow dynamics. For adult porcine hearts, only 0° and 15° apical twists were examined, the latter being the average maximum apical twist observed in adult human LVs (Sengupta et al., 2008).

2.7. Viscous energy loss analysis

Viscous frictional energy losses experienced by fluid moving through the heart was quantified according to previous methods (Vasudevan et al., 2017), for all the simulated hearts.

$$EL_{period} = \mathrm{W}_{\mathrm{period}} - KE_{out,period} - \Delta\mathrm{KE}_{\mathrm{period}} \tag{3}$$

$$\widehat{E} = \frac{\mathrm{EL\ for\ 1\ cycle}}{Stroke\ \ Volume} \tag{4}$$

Energy loss (EL_{period}) for a certain period (e.g. systole) was calculated via laws of conservation of energy, i.e., work done by LV wall on the fluid within the heart ($\mathrm{W}_{\mathrm{period}}$) less the outgoing kinetic energy ($KE_{out,period}$) and the increase in the kinetic energy of the fluid ($\Delta\mathrm{KE}_{\mathrm{period}}$). During diastole, appropriate negative signs would apply, such as on$\mathrm{W}_{\mathrm{period}}$, as work would be done by fluid on the cardiac wall. The total energy loss over one cardiac cycle was normalised by the stroke volume to yield the specific energy loss ($\widehat{E}$). It reflected the energy loss per unit volume of cardiac output pumped by the heart in a cardiac cycle, and was a measure of the energy efficiency of flow transiting through the heart, or the "flow energy efficiency". These energy terms reflected only the work done to overcome viscous energy losses experienced by the flow, and did not include work done to overcome afterload. Kinetic energy and work done terms were further defined as:

$$W_{period} = \int_{period}\int_{A_{wall}} P\left(\vec{v}.\hat{n}\right)dAdt \tag{5}$$

$$KE_{out,period} = \int_{period}\int_{A_{inlet}orA_{outlet}} \frac{1}{2}\rho v^2\left(\vec{v}.\hat{n}\right)dAdt \tag{6}$$

$$\Delta\mathrm{KE}_{period} = \left(\int_{V_{LV}} \frac{1}{2}\rho v^2 dV\right)\Bigg|\begin{matrix} t = t_{end} \\ t = t_{start}\end{matrix} \tag{7}$$

where, ρ was the density, $\vec{v}$ was the velocity vector, $\hat{n}$ was unit normal to surface boundary, P was fluid pressure, and t_{start} and t_{end} were time points at the beginning and end of the period. A_i was the surface area of the locale "i", while $\mathrm{V_{LV}}$ was the LV volume.

Average KE density, $\overline{KE}$, was the KE per unit LV volume averaged over a time period, and $\overline{WSS}$ was the time- and surface-averaged Wall Shear Stress (WSS) over a cardiac cycle. $\widehat{W}_{systole}$ was systolic work done normalized by the stroke volume. These were calculated as:

$$\overline{KE}_{\mathrm{period}} = \frac{1}{T_{period}}\int_{T_{period}}\left[\frac{1}{V_{LV}}\int_{V_{LV}}\frac{1}{2}\rho v^2 dV\right]dt \tag{8}$$

$$\overline{WSS} = \frac{1}{T}\int_{T}\left[\frac{1}{A_{wall}}\int_{A_{wall}}\mu\frac{\partial|\vec{v}|}{\partial\hat{n}}dA\right]dt \tag{9}$$

$$\widehat{W}_{systole} = \frac{\mathrm{W}_{systole}}{StrokeVolume} \tag{10}$$

3. Results

3.1. Physiological details of segmented foetal and porcine hearts

Physiological parameters of the simulated foetal and porcine hearts are given in Table 1. The two foetal subjects were named F#1 and F#2, while the five porcine subjects were named P#1 to P#5. Simulation cases where a rudimentary mitral valve was included were appended with "+MV" label, while cases where papillary muscles were included were appended with "+PM" label. The two porcine cases with induced MI were appended as "W_1" and "W_4" for acute and chronic time-points, respectively. Cases without papillary muscles generally had greater volumes, stroke volumes and cardiac outputs, as the papillary muscles were protrusions into the cardiac lumen. The inclusion of mitral valves, however, had minimal impact on the physiology of the hearts. The changes in physiology due to induced MI are also included in Table 1, and their effects on LV flow and energy dynamics has been studied in detail in our earlier work (Vasudevan et al., 2017). As seen from Table 1, foetal hearts were two orders of magnitudes smaller than adult hearts, while beating at more than 1.5 times the heart rate. Inter-subject variability between the foetal cases (in terms of ejection fraction and cardiac output), and between the adult cases (in terms of heart rate and cardiac output) were observed.

Figs. 2–4 show the flow simulation results in the form of vorticity iso-surfaces, calculated based on λ_2 criterion (Jeong and Hussain, 1995), and wall shear stress (WSS) surface contour plots. Results for porcine subjects P#1 and P#5 are shown in Figs. 2 and 3, respectively, while, those for human foetal subjects are shown in Fig. 4. From the figures, which list cases with and without ventricular torsional motions side-by-side, it was be observed that in all cases investigated, there were only minor differences in the vorticity dynamics and WSS patterns, both spatially and temporally.

Figs. 2–4 also demonstrated that prominent vortex structures in the form of shear layers on ventricular walls, and a pair of simple vortex rings corresponding to the E- and A-wave, were observed in the simulated LVs. Higher WSS were observed in the vicinity of the vortex rings as they brought faster moving flow near the LV wall. These observations agreed with our previous studies in the foetal (Lai et al., 2016; Wiputra et al., 2016) and adult hearts (Vasudevan et al., 2017). Due to inter-subject variability in LV geometry and physiological parameters (heart rate and stroke volume), significant differences in the vortex structures could be discerned between the foetal subjects and also between the porcine subjects, which was also in agreement with our previous study (Vasudevan et al., 2017). Vorticity dynamics appeared to be less complex in the foetal hearts due to a much lower Reynolds number.

Table 2 lists the calculated values of various energy indices at different degrees of torsional motion for both adult and foetal cases. Presence of the mitral valve increased the complexity of flow, as could be observed from the higher density of vortex structures (Figs. 2–4), leading to higher KE density, energy losses and WSS (Table 2). From the simulation results, it could also be observed that with the mitral valve, the penetration depth of the incoming mitral flow jet increased (Figs. 2–4), which brought fast moving fluid in the vortices closer to the walls. These results

Table 1
Physiological parameters of various foetal and porcine heart simulation cases. F#1 and F#2 were the 2 foetal LV, while P#1 - P#5 were the 5 porcine adult hearts. "+MV" and " +PM" indicate inclusion of the mitral valve and the papillary muscles, respectively, while "W_1" and "W_4" indicate the acute and chronic MI simulation cases.

		Heart Rate (bpm)	End-Diastolic Volume (EDV) (ml)	End-Systolic Volume (ESV) (ml)	Ejection Fraction (%)	Cardiac Output (L/min)
Adult Porcine LVs	P#1	63	91.5	44.3	51.6	2.98
	P#2	66	94.8	44.9	52.6	3.30
	P#3	68	105.6	52.4	50.4	3.62
	P#4	70	99.1	41.9	57.7	4.00
	P#5	87	111.2	49.8	55.3	5.32
	P#1 + MV	63	91.8	44.4	51.7	2.99
	P#2 + MV	66	94.8	44.9	52.6	3.30
	P#3 + MV	68	105.1	52.3	50.2	3.59
	P#4 + MV	70	99.1	41.9	57.7	4.00
	P#1 W_1	93	135.6	73.1	46.1	5.84
	P#1 W_4	95	94.9	61.0	35.7	3.23
	P#2 W_1	94	111.9	56.4	50.0	5.19
	P#2 W_4	65	106.9	59.0	44.8	3.12
	P#1 W_1 + MV	93	135.6	73.1	46.1	5.84
	P#1 W_4 + MV	95	95.0	60.6	34.5	3.27
	P#2 W_1 + MV	94	112.0	56.4	49.6	5.19
	P#2 W_4 + MV	65	106.9	59.0	44.8	3.12
	P#5 + PM	87	105.0	47.4	54.8	4.98
	P#5 + PM + MV	87	105.0	47.4	54.8	4.98
Human Foetal LV	F#1	147	0.98	0.34	65.6	0.094
	F#1 + MV	147	0.96	0.33	65.6	0.093
	F#2	147	0.72	0.31	57.0	0.056
	F#2 + MV	147	0.70	0.32	54.5	0.056

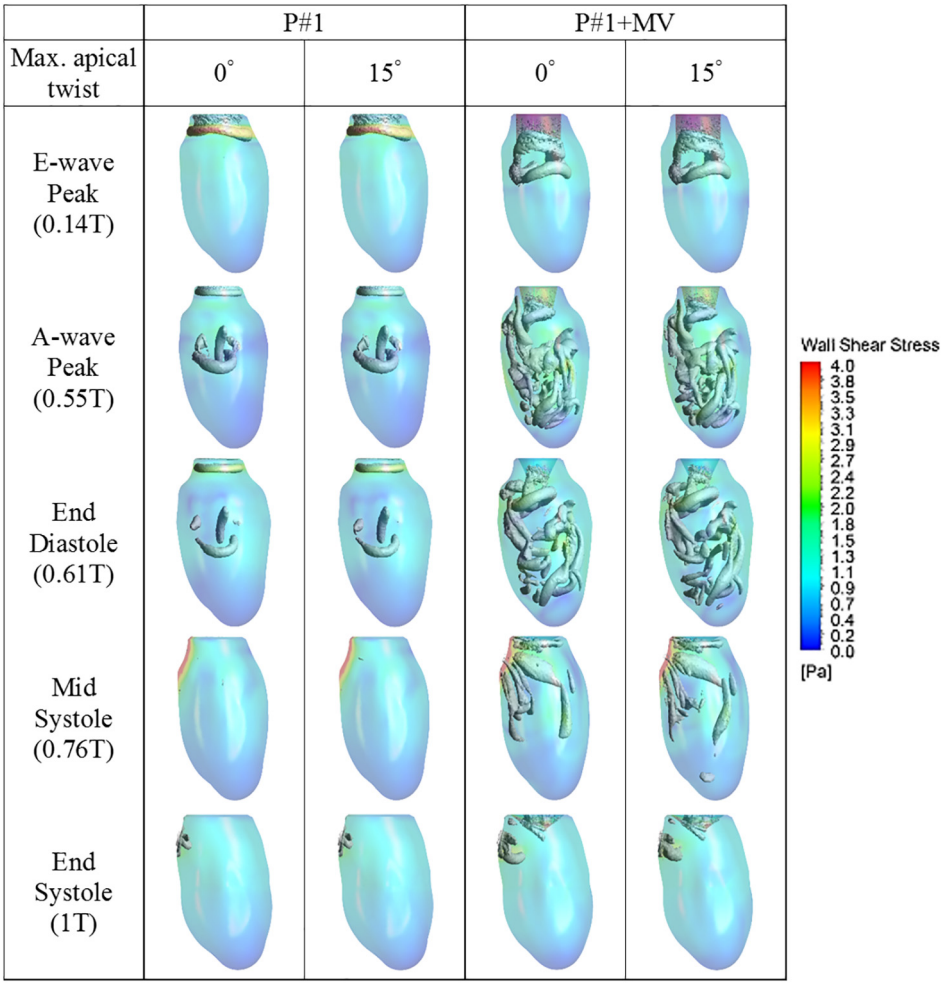

Fig. 2. Plot of vorticity iso-surfaces (λ_2 criterion of $-400\ s^{-2}$) and WSS colour contours at various time points in the cardiac cycle, demonstrating vortex rings forming in the porcine LV (subject #1), and generating elevated WSS on the wall close to them.

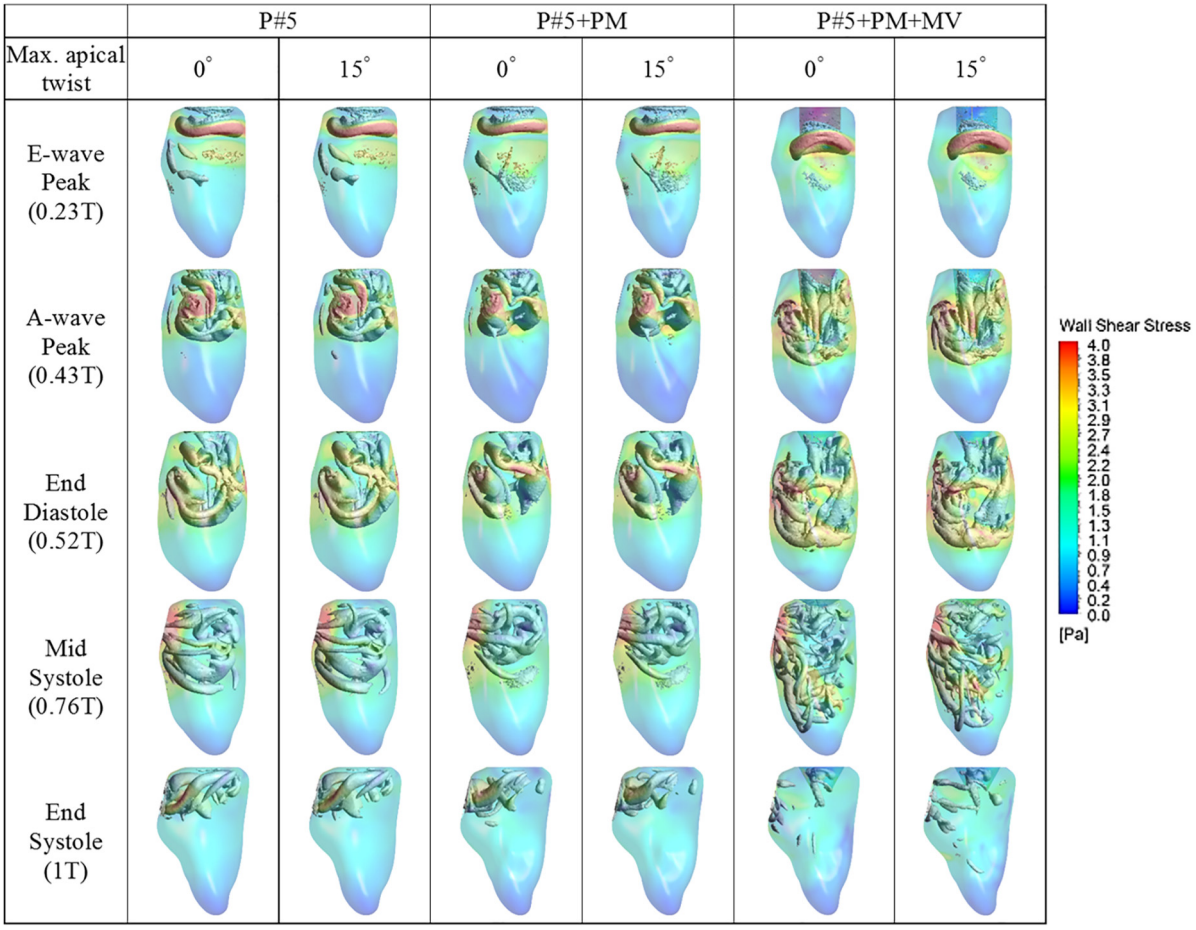

Fig. 3. Plot of vorticity iso-surfaces (λ_2 criterion of $-400\ s^{-2}$) and WSS colour contours at various time points in the cardiac cycle, demonstrating vortex rings forming in the porcine LV (subject #5), and generating elevated WSS on the wall close to them.

agreed with previous studies on the effects of mitral valve on LV flow patterns (Seo et al. 2014). There was, however, only a marginal change in the work required for systolic ejection between the cases with or without mitral valves. This was consistent with our earlier findings (Vasudevan et al., 2019) where we investigated the effect of diastolic vortices on the flow and energy dynamics during systolic ejection.

We observed that the energy indices changed very little between cases with and without torsion, as well as across various torsion extents investigated for the foetal hearts. Changes to flow energy losses, wall shear stresses and systolic ejection work done were consistently less than 2%, with or without ventricular torsion. The largest change (2.5%) was for the kinetic energy within the LV for case F#2+MV. Thus, the effect of wall torsion on flow dynamics was still small in all the cases investigated.

As found in our earlier study (Vasudevan et al., 2017), the flow and energy dynamics were substantially more sensitive to physiological parameters such as heart rate, LV size and stroke volume. For example, P#5 had a higher heart rate than P#1, and was associated with elevation of all energy measures. Further, P#5 had a lower stroke volume than P#5+PM, thus resulting in reduction of energy measures. The same could be observed for cases F#1 and F#2, consequent to the higher stroke volume in F#1.

Table 3 shows the p-values (calculated by two-sided Wilcoxon signed ranked test at 5% significance level) that indicate the statistical significance of the differences in the energy indices in the presence and absence of twist, with the null hypothesis being that there is no difference between the energy indices at the two twist conditions. The statistical analysis was performed only for the porcine subjects, as there were very few foetal subjects to conduct a meaningful statistical analysis. The high p-values are a result of a low sample size, and hence, there is not enough statistical evidence to reject the null hypothesis, suggesting that LV twist did not affected these energy and flow dynamics parameters. A significantly higher sample size might be required for a better statistical judgement on the null hypothesis. Nevertheless, in our opinion, the presence or absence of statistical significance might be unimportant, because in either case, the differences in energy indices would remain small for all the cases considered. (5 healthy cases and 4 diseased cases without MV, and the corresponding cases with MV, as well as two foetal cases with and without MV). The energy indices were far more dependent on changes in physiology (due to inter-subject variability and/or diseased conditions such as MI), and the presence of MV.

Overall, the results indicated that LV twist played a minimal role in the fluid and energy dynamics of blood flow through the left ventricles of adult and foetal hearts. This was observed in all the cases investigated irrespective of the presence or absence of papillary muscles and mitral valves, as well as in cases with myocardial infarction.

4. Discussion

In the current study, we performed extended studies on the effect of LV torsional motion on the flow and energy dynamics of

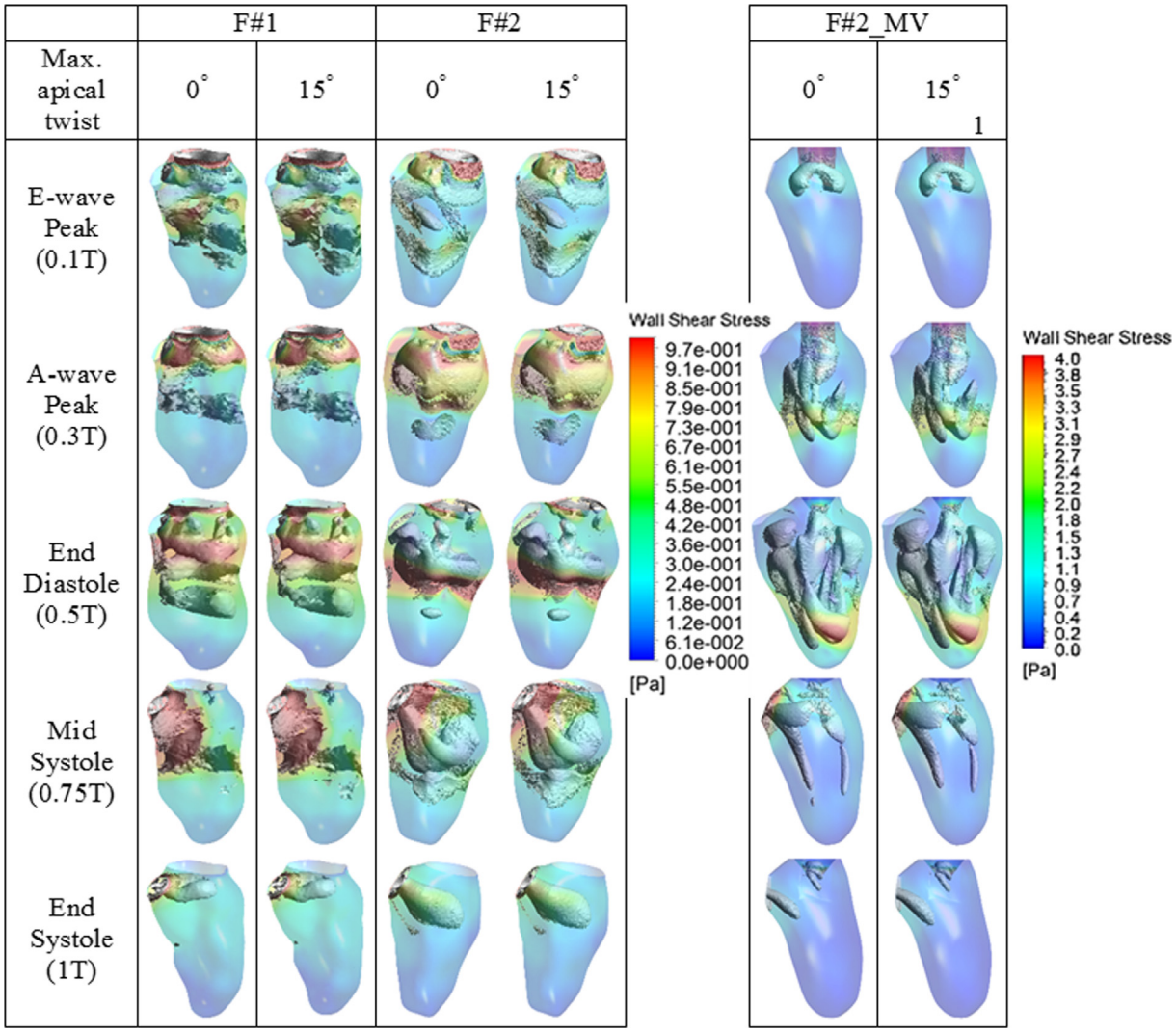

Fig. 4. Plot of vorticity iso-surfaces (λ_2 criterion of $-50\ s^{-2}$ for F#1 and F#2 case, and $-400\ s^{-2}$ for F#2+MV) and WSS colour contours at various time points in the cardiac cycle, demonstrating vortex rings formation and the subsequent elevation of WSS on the wall close to them.

the LV, using image-based CFD. Our investigations covered two different size scales, viz. human foetal hearts and adult porcine hearts, and included cases with and without the mitral valve and the papillary muscles. Two porcine cases with acute and chronic MI were also included in the study. Results demonstrated that at a realistic maximum ventricular torsion, estimated to be 15°, between the apex and the base of the heart, there were insignificant changes to the flow patterns and energy dynamics of flow in the heart. In fact, the resulting vorticity and wall shear stress plots were remarkably similar, suggesting that there were no specific regions in the LV where there were elevated differences caused by the torsion, and the differences were small everywhere.

The reason we investigated situations with and without the papillary muscles, was that the papillary muscles were protrusions into the LV lumen, and they could conceivably induce greater torsional flow. The mitral valve, on the other hand, was a more important consideration, as it increased mitral inflow velocities and deepened their penetration towards the apex, and caused vortices to have increased interactions with walls. Lastly, two porcine cases at different stages of MI were also included, as MI is known to significantly affect the LV physiology (Table 1) (Kupper et al., 1977; Nager et al., 1967). LV torsion had little direct consequence on the fluid mechanics of the LV, in the sense that the lateral shear induced by the torsional motion only brought about small changes in the flow. This was approximated to be 2 orders of magnitude smaller than the momentum energy of cardiac flows, given that the torsion only brought about less than 2% change in energy parameters. Results, demonstrated that papillary muscles and mitral valves were not important to the effect of torsion motion on flow dynamics.

Our current and previous simulations (Vasudevan et al., 2017) indicated that physiological parameters such as heart rate, stroke volume, ventricular anatomy and size had much greater influence on flow patterns and energy dynamics. To date, there have been a number of simulations of the LV fluid dynamics (Domenichini et al., 2005; Lai et al., 2016; Larsson et al., 2017; Mihalef et al., 2011; Schenkel et al., 2009; Seo et al., 2014; Su et al., 2014; Vedula et al., 2016; Wiputra et al., 2017), which did not include modelling of LV torsion. Our study demontrated that the lack of LV torsion would not have significantly affected the results, and future simulations may not need to model the torsion.

Clinically, however, the LV torsion is known to correlate cardiac hemodynamics and heart function (Pacileo et al., 2011; Tan et al., 2009). This could be explained by the LV torsion being an indicator of the contractility and manner of contraction of the heart, which were the primary determininats of the hemodynamic outcome.

Table 2
Energy indices for adult porcine (P#1 - P#5) and human foetal (F#1 and F#2) left ventricles at different degrees of maximum apical twist. $\widehat{E}$ – Energy loss per cycle per cardiac output, KE – time-averaged kinetic energy density, WSS – time- and space-averaged wall shear stress, $\widehat{W}_{syst.}$ – work done for systolic ejection per stroke volume. "+PM" indicates inclusion of papillary muscles in the simulations, while "+MV" indicates inclusion of the mitral valve in the simulations. "W_1" and "W_4" indicate the acute and chronic MI cases. % change was calculated based on comparison with the corresponding 0° twist case, which is the absence of ventricular torsion.

	Case	Max. apical twist (ε)	$\widehat{E}$(mJ/L)		$\overline{KE}$(mJ/L)		$\overline{WSS}$(Pa)		$\widehat{\widehat{W}}_{systole}$(mJ/L)	
				% change		% change		% change		% change
Adult Porcine LV	P#1	0°	49.6		7.73		0.823		1102	
		15°	49.5	−0.2%	7.75	0.3%	0.826	0.4%	1106	0.4%
	P#2	0°	100.4		15.77		1.176		752	
		15°	100.8	0.4%	15.82	0.3%	1.178	0.2%	754	0.3%
	P#3	0°	35.36		9.40		0.872		256.0	
		15°	35.30	−0.2%	9.42	0.2%	0.876	0.5%	256.3	0.1%
	P#4	0°	87.0		15.25		1.122		2041	
		15°	86.6	−0.5%	15.27	0.1%	1.123	0.1%	2046	0.2%
	P#5	0°	73.62		23.9		1.37		563.7	
		15°	73.55	−0.1%	23.8	−0.4%	1.36	−0.7%	564.2	0.1%
	P#1 + MV	0°	112.9		15.60		1.12		1144	
		15°	111.7	−1.1%	15.57	−0.2%	1.13	0.9%	1134	−0.9%
	P#2 + MV	0°	294.6		28.7		1.497		738	
		15°	295.0	0.1%	28.8	0.6%	1.503	0.4%	740	0.3%
	P#3 + MV	0°	89.4		17.7		1.165		250	
		15°	88.6	−0.9%	17.6	−0.5%	1.162	−0.3%	249	−0.4%
	P#4 + MV	0°	195.8		27.51		1.489		2077	
		15°	196.1	0.2%	27.46	−0.2%	1.486	−0.2%	2075	−0.1%
	P#1 W_1	0°	166.99		26.69		1.477		1765	
		15°	166.96	−0.02%	26.71	0.1%	1.482	0.3%	1762	−0.2%
	P#1 W_4	0°	81.2		13.07		1.027		934	
		15°	82.1	1.1%	13.28	1.6%	1.033	0.6%	947	1.4%
	P#2 W_1	0°	148.9		29.2		1.571		3464	
		15°	146.9	−1.3%	29.1	−0.3%	1.576	0.3%	3446	−0.5%
	P#2 W_4	0°	90.5		14.42		1.114		1202.1	
		15°	90.6	0.1%	14.44	0.1%	1.117	0.3%	1201.8	−0.02%
	P#1 W_1 + MV	0°	508.1		61.8		2.211		1731	
		15°	508.0	−0.02%	61.3	−0.8%	2.208	−0.1%	1725	−0.4%
	P#1 W_4 + MV	0°	176		25.3		1.334		973	
		15°	179	1.7%	25.7	1.7%	1.342	0.6%	980	0.7%
	P#2 W_1 + MV	0°	386		52.7		2.078		3422	
		15°	381	−1.2	51.9	−1.5%	2.082	0.2%	3395	−0.8%
	P#2 W_4 + MV	0°	311		27.2		1.473		1192	
		15°	313	0.5%	27.3	0.2%	1.472	−0.1%	1193	0.1%
	P#5 + PM	0°	64.1		20.04		1.287		400	
		15°	63.8	−0.5%	20.05	0.00%	1.289	0.2%	401	0.3%
	P#5 + PM + MV	0°	136		29.5		1.54		396	
		15°	139	1.8%	29.9	1.4%	1.56	1.3%	397	0.4%
Human Foetal LV	F#1	0°	26.01		2.901		0.701		181.1	
		5°	25.99	−0.1%	2.899	−0.1%	0.701	0.0%	180.6	−0.3%
		10°	26.02	0.0%	2.903	0.1%	0.702	0.1%	180.7	−0.2%
		15°	26.01	0.0%	2.901	0.0%	0.702	0.1%	180.5	−0.3%
	F#1 + MV	0°	68.6		5.50		0.911		173.2	
		15°	69.9	1.9%	5.61	2.0%	0.925	1.5%	174.9	1.0%
	F#2	0°	22.85		2.130		0.562		85.1	
		5°	22.81	−0.2%	2.128	−0.1%	0.562	0.0%	85.0	−0.1%
		10°	22.78	−0.3%	2.124	−0.3%	0.562	0.0%	85.0	−0.1%
		15°	22.75	−0.4%	2.121	−0.4%	0.563	0.2%	84.9	−0.2%
	F#2 + MV	0°	60.3		4.04		0.73		81.4	
		15°	61.4	1.8%	4.14	2.5%	0.74	1.9%	82.3	1.1%

Table 3
p-values (at 5% significance level) from two-sided Wilcoxon signed rank test to indicate statistical significance of differences in energy indices between the porcine hearts at the two twist conditions investigated (0° and 15°). "Healthy + Disease" indicates that the 4 cases of infarcted heart simulations were grouped with the 5 cases of healthy heart simulations to make n = 9. * indicates that the P#5 + PM + MV case was used as one "with MV" case, grouped with other cases where the PM was not modelled.

p-value	n	$\Delta\widehat{E}$	$\Delta\overline{KE}$	$\Delta\overline{WSS}$	$\Delta\widehat{\widehat{W}}_{systole}$
Healthy (with no MV)	5	0.50	0.56	0.63	0.06
Healthy (with MV)	5*	1.00	0.88	0.31	0.69
Healthy + Diseased (with no MV)	9	0.71	0.43	0.12	0.44
Healthy + Diseased (with MV)	9*	0.71	0.88	0.16	0.45

The direct contribution of the shearing motion of the ventricular torsion to fluid motion, such as that tested in the current study, would be difficult to test clinically.

The current study has a few limitations. Firstly, the ventricular twist was modelled as a net basal-to-apical twist, that increased linearly from zero at the base to a maximum at the apex, while in the actual heart, the base twisted in a direction opposite to that at the apex. However, our modelling could be argued to be a more extreme test case, as we would have larger amplitudes of torsional wall velocities as opposed to the situation where some parts of the heart were twisting in an opposite direction. Modelling the opposite twist at the base would only reduce the contribution of ventricular torsion to flow dynamics. Secondly, we did not test cases where mitral valve chords were present. Since these chords transverse the ventricular lumen, they could bring about greater torsional forces on the blood fluid. Thirdly, our mitral valve model was a simplified and rudimentary one, and would be sufficiently accurate to represent the actual fluid-interaction between the valve and flow. However, this was not the focus of our study. The mitral valve model achieved the desired effects of narrowing and accelerating the inflow as a mitral valve should, and enabled us to test the effects of ventricular torsion under such a cardiac flow condition. Finally, we performed a statistical analysis on a limited number of porcine subjects, and more subjects might be required to make better statistical inference. However, our simulations showed that the effect of twist on LV energetics was very small (by about 2 orders of magnitude) compared to the effects of changes in physiology.

5. Conclusion

We performed simulations of flow in the left ventricle at the foetal and adult length scales, without and without papillary muscles and mitral valves, as well as under a diseased condition, to investigate whether ventricular torsion affected flow and energy dynamics. We found that ventricular torsion had insignificant direct influence on flow patterns, energy losses, ejection work done and wall shear stress. Therefore, excluding torsion from LV simulation models would not significantly affect the fluid dynamics.

Acknowledgement

We thank the National University of Singapore (NUS) Young Investigator Award (2015, PI: Yap), and Singapore Ministry of Education Grant #MOE2018-T2-1-003 for funding, and the NUS Graduate School of Integrated Sciences for scholarship support for the lead author. All authors have no conflict of interest to declare.

Declaration of Competing Interest

All authors have no conflict of interest to declare.

Appendix A. Supplementary material

Supplementary data to this article can be found online at https://doi.org/10.1016/j.jbiomech.2019.109357.

References

Buckberg, G.D., Hoffman, J.I., Coghlan, H.C., Nanda, N.C., 2015. Ventricular structure-function relations in health and disease: Part I. The normal heart. Eur J Cardiothorac Surg 47, 587–601.

Domenichini, F., Pedrizzetti, G., Baccani, B., 2005. Three-dimensional filling flow into a model left ventricle. J. Fluid Mech. 539, 179–198.

Elbaz, M., Calkoen, E.E., Westenberg, J., Lelieveldt, B., Roest, A., van der Geest, R.J., 2014. Vortex flow during early and late left ventricular filling in normal subjects: quantitative characterization using retrospectively-gated 4D flow cardiovascular magnetic resonance and three-dimensional vortex core analysis. J. Cardiovasc. Magn. Reson. 16, 78.

Grosberg, A., Gharib, M., 2009. Computational models of heart pumping efficiencies based on contraction waves in spiral elastic bands. J. Theor. Biol. 257, 359–370.

Jeong, J., Hussain, F., 1995. On the identification of a vortex. J. Fluid Mech., 285

Kupper, W., Bleifeld, W., Hanrath, P., Mathey, D., Effert, S., 1977. Left ventricular hemodynamics and function in acute myocardial infarction: studies during the acute phase, convalescence and late recovery. Am. J. Cardiol. 40, 900–905.

Kunzelman, K.S., Cochran, R.P., Verrier, E.D., Eberhart, R.C., 1994. Anatomic basis for mitral valve modelling. J. Heart Valve Dis. 3, 491–496.

Lai, C.Q., Lim, G.L., Jamil, M., Mattar, C.N., Biswas, A., Yap, C.H., 2016. Fluid mechanics of blood flow in human fetal left ventricles based on patient-specific 4D ultrasound scans. Biomech. Model Mechanobiol. 15, 1159–1172.

Larsson, D., Spuhler, J.H., Petersson, S., Nordenfur, T., Colarieti-Tosti, M., Hoffman, J., Winter, R., Larsson, M., 2017. Patient-specific left ventricular flow simulations from transthoracic echocardiography: robustness evaluation and validation against ultrasound doppler and magnetic resonance imaging. IEEE Trans. Med. Imaging 36, 2261–2275.

Li, Y., Sun, J., Tang, C.-K., Shum, H.-Y., Year Lazy snapping. In ACM Transactions on Graphics (ToG).

Mihalef, V., Ionasec, R.I., Sharma, P., Georgescu, B., Voigt, I., Suehling, M., Comaniciu, D., 2011. Patient-specific modelling of whole heart anatomy, dynamics and haemodynamics from four-dimensional cardiac CT images. Interf. Focus 1, 286–296.

Nakatani, S., 2011. Left ventricular rotation and twist: why should we learn?. J. Cardiovasc. Ultrasound. 19, 1–6.

Nager, F., Thomas, M., Shillingford, J., 1967. Changes in cardiac output and stroke volume during first four months after cardiac infarction. Br. Heart J. 29, 859–870.

Pacileo, G., Baldini, L., Limongelli, G., Di Salvo, G., Iacomino, M., Capogrosso, C., Rea, A., D'Andrea, A., Russo, M.G., Calabro, R., 2011. Prolonged left ventricular twist in cardiomyopathies: a potential link between systolic and diastolic dysfunction. Eur. J. Echocardiogr. 12, 841–849.

Pedrizzetti, G., La Canna, G., Alfieri, O., Tonti, G., 2014. The vortex [mdash] an early predictor of cardiovascular outcome?. Nat. Rev. Cardiol. 11, 545–553.

Schenkel, T., Malve, M., Reik, M., Markl, M., Jung, B., Oertel, H., 2009. MRI-based CFD analysis of flow in a human left ventricle: methodology and application to a healthy heart. Ann. Biomed. Eng. 37, 503–515.

Sengupta, P.P., Krishnamoorthy, V.K., Korinek, J., Narula, J., Vannan, M.A., Lester, S.J., Tajik, J.A., Seward, J.B., Khandheria, B.K., Belohlavek, M., 2007. Left ventricular form and function revisited: applied translational science to cardiovascular ultrasound imaging. J. Am. Soc. Echocardiogr. 20, 539–551.

Sengupta, P.P., Tajik, A.J., Chandrasekaran, K., Khandheria, B.K., 2008. Twist mechanics of the left ventricle: principles and application. JACC Cardiovasc. Imaging 1, 366–376.

Seo, J.H., Vedula, V., Abraham, T., Lardo, A.C., Dawoud, F., Luo, H., Mittal, R., 2014. Effect of the mitral valve on diastolic flow patterns. Phys. Fluids 26, 121901.

Su, B., Zhang, J.-M., Tang, H.C., Wan, M., Lim, C.C.W., Su, Y., Zhao, X., Tan, R.S., Zhong, L., 2014. Patient-specific blood flows and vortex formations in patients with hypertrophic cardiomyopathy using computational fluid dynamics. In: 2014 IEEE Conference on Biomedical Engineering and Sciences (IECBES), pp. 276–280.

Taber, L.A., Yang, M., Podszus, W.W., 1996. Mechanics of ventricular torsion. J. Biomech. 29, 745–752.

Tan, Y.T., Wenzelburger, F., Lee, E., Heatlie, G., Leyva, F., Patel, K., Frenneaux, M., Sanderson, J.E., 2009. The pathophysiology of heart failure with normal ejection fraction: exercise echocardiography reveals complex abnormalities of both systolic and diastolic ventricular function involving torsion, untwist, and longitudinal motion. J Am Coll Cardiol 54, 36–46.

Vasudevan, V., Low, A.J.J., Annamalai, S.P., Sampath, S., Poh, K.K., Totman, T., Mazlan, M., Croft, G., Richards, A.M., de Kleijn, D.P., Chin, C.L., Yap, C.H., 2017. Flow dynamics and energy efficiency of flow in the left ventricle during myocardial infarction. Biomech. Model. Mechanobiol. 16, 1503–1517.

Vasudevan, V., Low, A.J.J., Annamalai, S.P., Sampath, S., Chin, C.L., Ali, A.A.B., Yap, C. H., 2019. Role of diastolic vortices in flow and energy dynamics during systolic ejection. J. Biomech. 90, 50–57.

Vedula, V., Seo, J.-H., Lardo, A.C., Mittal, R., 2016. Effect of trabeculae and papillary muscles on the hemodynamics of the left ventricle. Theor. Comput. Fluid Dyn. 30, 3–21.

Wiputra, H., Lai, C.Q., Lim, G.L., Heng, J.J.W., Guo, L., Soomar, S.M., Leo, H.L., Biwas, A., Mattar, C.N.Z., Yap, C.H., 2016. Fluid mechanics of human fetal right ventricles from image-based computational fluid dynamics using 4D clinical ultrasound scans. American J. Physiol. Heart Circulat. Physiol. 311, H1498–H1508.

Wiputra, H., Lim, G.L., Chua, K.C., Nivetha, R., Soomar, S.M., Biwas, A., Mattar, C.N.Z., Leo, H.L., Yap, C.H., 2017. Peristaltic-like motion of the human fetal right ventricle and its effects on fluid dynamics and energy dynamics. Ann. Biomed. Eng., 1–13

Zhang, Y., Zhou, Q.C., Pu, D.R., Zou, L., Tan, Y., 2010. Differences in left ventricular twist related to age: speckle tracking echocardiographic data for healthy volunteers from neonate to age 70 years. Echocardiography 27, 1205–1210.